Ocean Dynamics (2003) 53: 1–10
DOI 10.1007/s10236-002-0015-6

Inga Hense · Ralph Timmermann · Aike Beckmann
Ulrich V. Bathmann

Regional and interannual variability of ecosystem dynamics in the Southern Ocean

Received: 4 December 2001 / Accepted: 23 July 2002

Abstract To investigate regional and interannual variability of the ecosystem in the Southern Ocean, a coupled circumpolar ice–ocean–plankton model has been developed. The ice–ocean component (known as BRIOS-2) is based on a modified version of the s-coordinate primitive equation model (SPEM) coupled to a dynamic–thermodynamic sea-ice model. The biological model (BIMAP) comprises two biogeochemical cycles – silica and nitrogen – and a prognostic iron compartment to include possible effects of micronutrient limitation. Simulations with the coupled ice–ocean–plankton model indicate that the physical–biological interaction is not limited to the effect of a varying surface mixed-layer depth. In the Pacific sector, large anomalies in winter mixed-layer depth cause an increased iron supply and enhance primary production and plankton biomass in the following summer, whereas in the Atlantic sector variability in primary production is caused mainly by fluctuations of oceanic upwelling. Thus, the Antarctic Circumpolar Wave (ACW) induces regional oscillations of phytoplankton biomass in both sectors, but not a propagating signal. Furthermore, interannual variability in plankton biomass and primary production is strong in the Coastal and Continental Shelf Zone and the Seasonal Ice Zone around the Antarctic continent. Interannual variability induced by the ACW has large effects on the regional scale, but the associated variability in biogenic carbon fluxes is small compared to the long-term carbon sequestration of the Southern Ocean.

Keywords ACW · Southern Ocean · Plankton biomass · Interannual variability · Coupled ice–ocean–ecosystem model

Responsible Editor: Andreas Oschlies

I. Hense (✉) · R. Timmermann · A. Beckmann · U. V. Bathmann
Alfred Wegener Institute for Polar and Marine Research,
Bremerhaven, Germany

Present address: I. Hense
Université Libre de Bruxelles,
Ecologie des Systèmes Aquatique, Brussels, Belgium
e-mail: ihense@ulb.ac.be

Present address: R. Timmermann
Institut d'Astronomie et de Géophysique G. Lemaître,
Université Catholique de Louvain,
Louvain-la-Neuve, Belgium

1 Introduction

The Antarctic Circumpolar Wave (ACW) is one of the prominent signals of interannual variability in the Southern Ocean (White and Peterson 1996).

Based on ECMWF reanalysis data along 56°S and on remote sensing sea-ice concentration data, the ACW has been described as a set of closely connected anomalies of sea-surface pressure and temperature, meridional wind stress and sea-ice extent. These patterns propagate around Antarctica with a predominantly 4-year period, typically featuring a quadrupole structure of positive and negative anomalies. They are linked to regional oscillations; quasiperiodic fluctuations of meridional wind stress in the Weddell Sea drive interannual variations of ice export and sea-ice formation (Timmermann et al. 2002b).

Oscillations in air–sea CO_2 fluxes related to the ACW have been deduced from the interannual variability of the mixed-layer depth in a global OGCM (Le Quéré et al. 2000). However, a systematic investigation of the ecosystem's response to quasiperiodic fluctuations in physical boundary conditions has not yet been performed.

To investigate the mechanisms relevant for regional interannual variability of primary production and plankton bloom development, a biological model of intermediate complexity (biological model for the antarctic plankton community, BIMAP) has been developed and coupled to the circumpolar ice–ocean model BRIOS-2 (Timmermann et al. 2002a). In this paper, we describe the model setup and analyze physical–biological interactions in different regions of the Southern Ocean.

2 Model setup

The coupled ice–ocean–ecosystem model presented here is based on the circumpolar ice–ocean model BRIOS-2 (Timmermann et al. 2002a) which consists of a modified version of the s-coordinate primitive equation model (SPEM; Haidvogel et al. 1991; Beckmann et al. 1999) and a dynamic–thermodynamic sea-ice model (Hibler 1979) and has been used succesfully in a number of regional climate-modelling and process study applications (Beckmann et al. 2001; Timmermann et al. 2002b). The model comprises the area south of 50°S and has a resolution of 1.5° in the Atlantic Sector of the Southern Ocean. More details of the physical model and its validation can be found in Timmermann et al. (2002a).

The ecosystem model (BIMAP) includes two biogeochemical cycles – silica and nitrogen – and considers possible micronutrient limitation. It comprises compartments for phyto- and zooplankton, the nutrients nitrate, ammonium, silicate and iron and two compartments for nitrogen- and silica-based detritus (see Appendix A). Silica, nitrogen and iron uptake are linked by constant factors. Parameterizations are derived from measurements mainly from Antarctic diatom and copepod species. The model considers advection and diffusion using velocities and diffusivities from the ocean model and does not explicitly assume a homogeneous surface mixed layer. Coupled to an eddy-resolving implementation of SPEM, it has been used and validated in an idealized configuration representing a section of the Antarctic Circumpolar Current (Hense et al., personal communication 2002) and shows good quantitative agreement with observations of phyto-/zooplankton and nutrient concentrations in that region.

The presence of sea ice influences the marine ecosystem mainly by the absorption of light, which reduces or prohibits primary production. In the coupled model, sea ice is assumed to absorb shortwave radiation in the photosynthetically active band with an extinction coefficient of 3 m^{-1}; total solar irradiance at the ocean surface is a weighted average over the ice-covered and open-water parts of each grid cell using the ice concentration A as a measure of fractional coverage.

The ocean model is initialized using data from the Hydrographic Atlas of the Southern Ocean (Olbers et al. 1992) and with zero ice volume. Initial silicate and nitrate fields are derived from the gridded WOCE data set (WOCE 1997); for ammonium, phyto- and zooplankton we chose typical winter concentrations of 0.1 μmol l^{-1}, 0.2 μg l^{-1} Chl a and 0.1 μg l^{-1} C. Due to the lack of reliable, gridded data, dissolved iron concentration is initialized with no horizontal gradients and a concentration increasing linearly with depth following observations from the Southern Ocean (Löscher et al. 1997; Sohrin et al. 2000; de Baar and de Jong 2001). Initial concentrations in the detritus pools are zero. The model is forced using 6-hourly wind fields, air and dew point temperatures, and cloudiness from the ECMWF reanalysis of 1985–1993 and the analysis of 1994–1999.

3 Results

Simulated climatological monthly means of phytoplankton distribution compare well with satellite data, taking into account the relatively coarse resolution of the model which cannot reproduce the observed mesoscale patchiness (Fig. 1, upper panels). During the period of maximum phytoplankton concentrations, in January, areas with enhanced phytoplankton biomass are found in the coastal and continental shelf zones, at the northern tip of the Antarctic Peninsula, east of South America and at some locations within the Seasonal Ice Zone (SIZ), especially in the Ross Sea. In the coastal areas, coastal upwelling leads to enhanced nutrient supply in the euphotic zone (Fig. 1, lower panels), which enables favourable growth conditions for phytoplankton in summer. High phytoplankton concentrations along the 50°S latitude in the Atlantic sector resemble the increased biomass near the Antarctic Polar Front. In this region near the northern boundary of the model domain, hydrography is strongly restored to observations and thus includes the pattern of the fronts. Cross-frontal circulation in this area features a persistent regional overturning which leads to a vertical redistribution of nutrients and thus to the development of a considerable phytoplankton bloom. This issue is addressed in more detail in a study with an eddy-resolving application of BIMAP (Hense et al., personal communication 2002).

In vast areas of the Southern Ocean, iron deficiency plays a major role in suppressing phytoplankton blooms: in the southern ACC, iron limitation causes a band with low chlorophyll concentrations, known as the high-nutrient low-chlorophyll (HNLC) area, which is well represented by the model. However, the extremely low iron concentration (<0.05 nmol l^{-1}) in some patches in the Pacific sector of the ACC might be slightly underestimated by the model as iron input by dust is not included (Fig. 1, bottom left). Besides silicate limitation in coastal regions with high phytoplankton concentrations (e.g. on the Patagonian Shelf), low silicate concentrations limit primary production in the open ocean north of the Antarctic Polar Front, which can be seen in the Pacific sector of the model domain (Fig. 1, bottom right). In the coastal zone of the Amundsen and Bellingshausen Seas, the model appears to underestimate phytoplankton concentrations. Most of this area is ice-covered even in summer, and oceanic primary production is confined to small polynyas near the coast which cannot be resolved by the model. Furthermore, local input of iron by dust or melting ice is not considered in the simulated concentration of dissolved iron. However, SeaWIFS data tend to heavily overestimate phytoplankton concentrations in coastal areas (e.g.

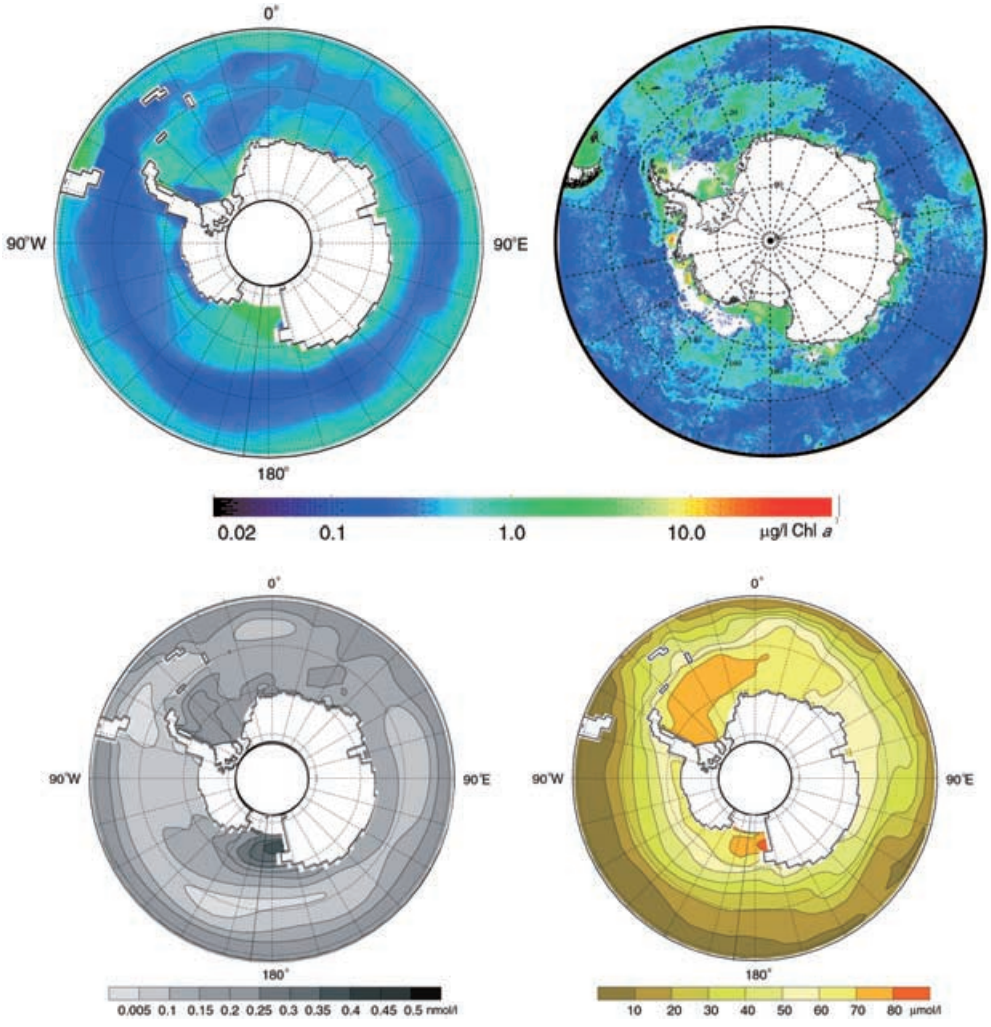

Fig. 1 Climatological monthly mean for January of surface phytoplankton concentration (µg Chl a l^{-1}) from a simulation with the coupled ice–ocean–ecosystem model (*top left*) and from a SeaWIFS image (1998–2000; Schwarz, personal communication *top right*), of simulated dissolved iron concentration (nmol l^{-1}) (*bottom left*) and simulated silicate concentration (*bottom right*)

Kudela and Chavez 1998; Kahru and Mitchell 1999); the distinction between sea ice and a phytoplankton bloom is not always certain. We conclude that the discrepancy between the simulation and the observations in this region is probably due to errors in both the model and the data.

High simulated phytoplankton concentration in the Ross Sea is caused by (1) an early start of phytoplankton bloom in the regularly occurring Ross Polynya, (2) a shallow surface mixed layer in summer (due to high input of sea-ice melt water) and (3) persistent oceanic upwelling (0.6 m day^{-1} in 100 m depth in the April–September mean) in winter, which ensures nutrient supply.

3.1 Variability in the southern ACC

Hovmoeller diagrams of the simulated sea-surface temperature (SST) averaged between 53 and 61°S (Fig. 2, top panel) show propagating anomalies consistent with the analyses of White and Peterson (1996) and the simulations of Beckmann and Timmermann (2001). Maximum amplitudes (±0.08 °C) are found in the Pacific Sector at roughly 140°W. Along with the SST, anomalies of mixed-layer depth feature a local period of about 3–4 years (Fig. 2, bottom panel), propagating eastward around the globe within 5–8 years, which is consistent with simulations of Le Quéré et al. (2000), who used an ocean model with 1.5-order turbulent closure scheme with an explicit formulation of the mixed layer. Propagating cold SST anomalies are generally associated with an anomalously deep mixed layer, but the highest amplitudes of mixed layer depth (±36 m) are localized in a standing wave pattern in the western Ross Sea sector (155°W). This is the region where the largest amplitudes of wind speed and heat flux variability are found; fluctuations of turbulent kinetic energy input caused by varying wind speed together with the interannual variability of surface heat fluxes create strong anomalies of mixed-layer depth.

The ecosystem's response to the interannual variability of physical boundary conditions is at first sight surprising: there is no obvious propagating signal in phytoplankton concentrations (Fig. 3, top panel). Corresponding to the variations of mixed-layer depth, the

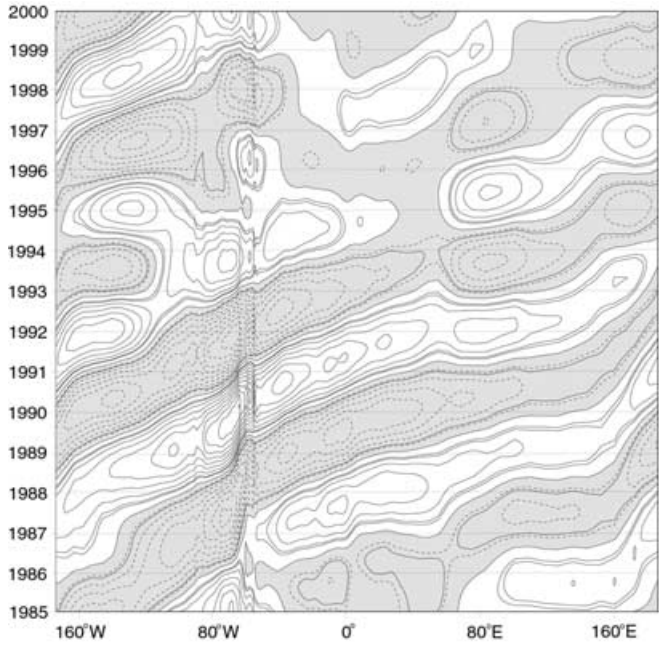

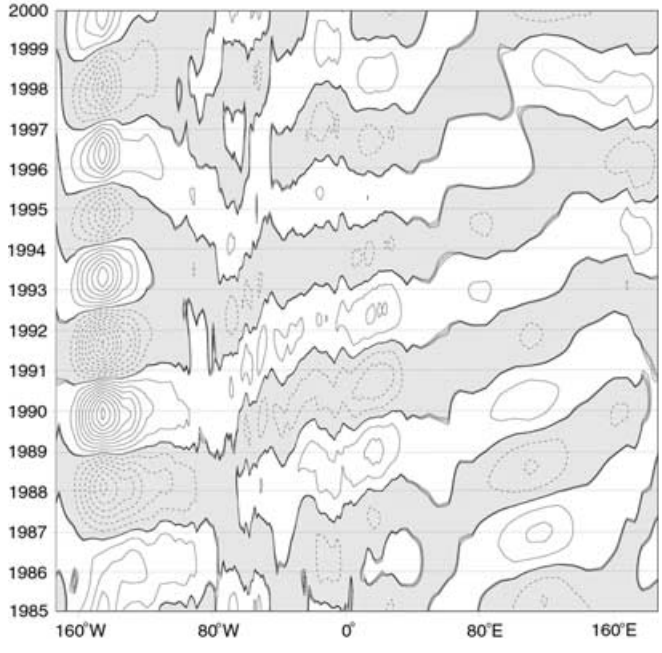

Fig. 2 Filtered anomalies (averaged over 53–61°S) of simulated SST (*top*) and mixed layer depth (*bottom*). Contour interval is 0.08°C for SST and 4 m for mixed layer depth. Negative values are *grey-shaded*. Data were filtered using a 3–7 year bandpass filter, as in the analysis of White and Peterson (1996)

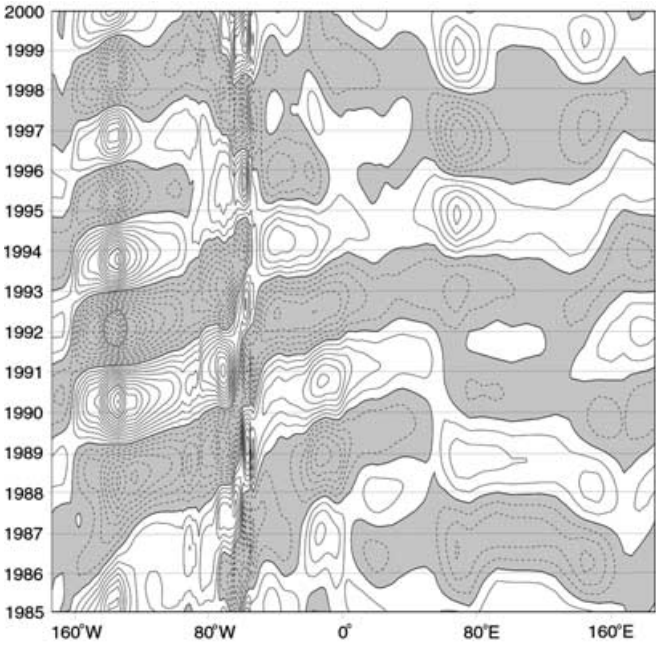

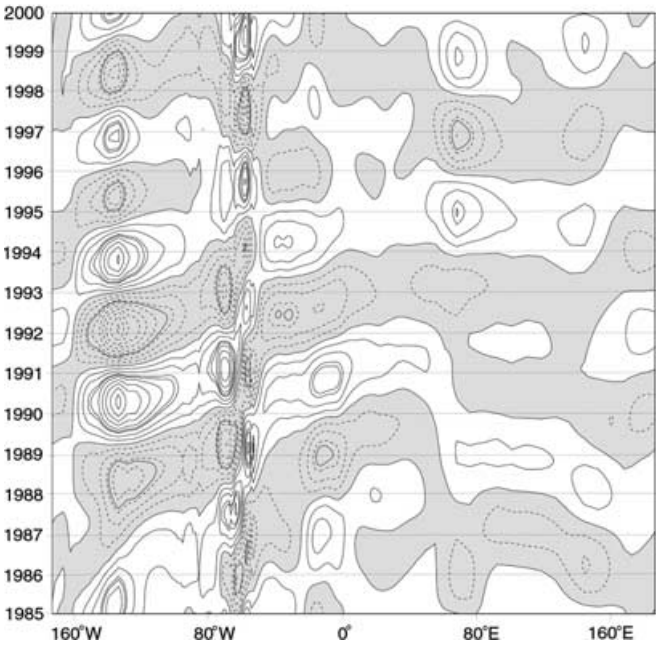

Fig. 3 Filtered anomalies (averaged over 53–61°S) of phytoplankton (*top*) and zooplankton (*bottom*) concentrations. Contour interval is 0.01 μg Chl al^{-1} for phytoplankton and 0.03 μg C l^{-1} for zooplankton. Negative values are *grey-shaded*. Data were filtered using a 3–7 year bandpass filter

largest anomalies of phytoplankton concentrations occur in the Pacific sector. Positive anomalies of phytoplankton concentrations are linked to positive anomalies of mixed-layer depth. While the variability of summer mixed-layer depth is small, positive anomalies of winter mixed-layer depth cause a higher input of iron (Fig. 4, top panel) which enhances phytoplankton growth in the subsequent spring and summer. Depending on the time of maximum mixed-layer depth, we find a time lag of about 3–5 months between the anomalies of mixed-layer depth and iron concentrations on the one hand and phytoplankton concentrations on the other. Consequently, negative anomalies of winter mixed-layer depth cause negative anomalies of iron entrainment, and thus lead to reduced phytoplankton concentrations in the following summer.

The characteristics of physical–biological interaction are different on the eastern side of the Antarctic

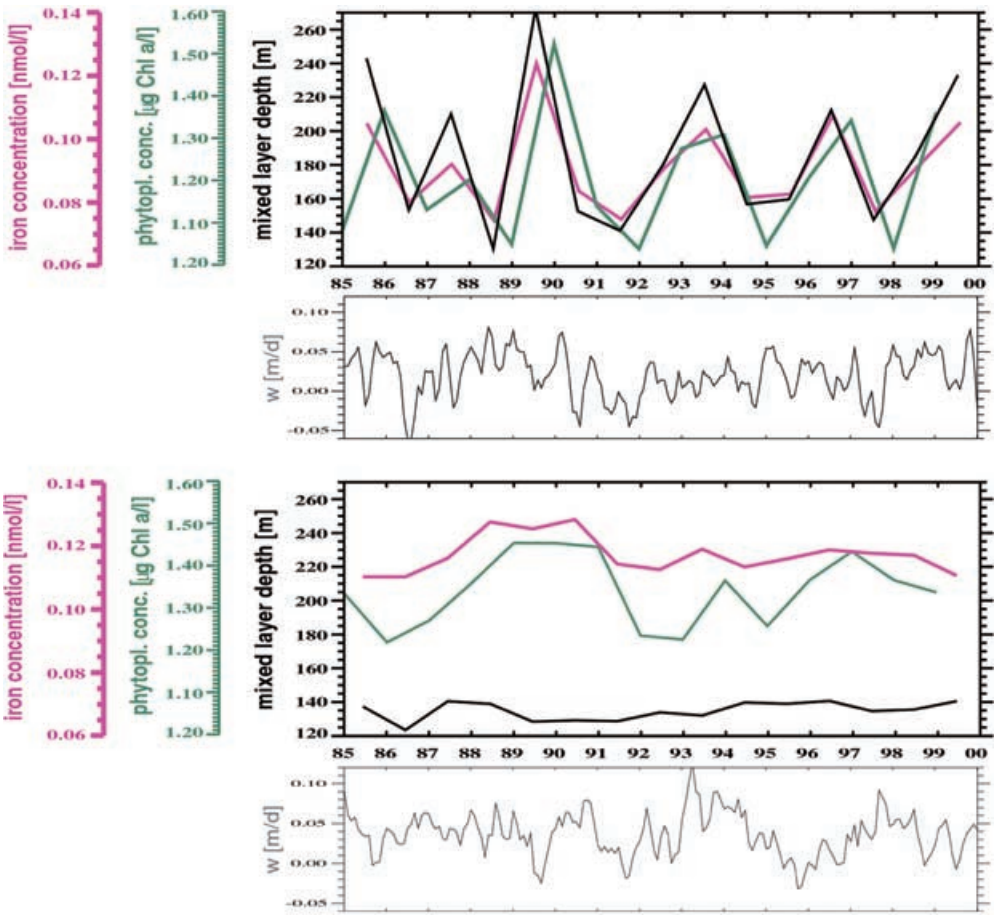

Fig. 4 Time series of the simulated maxima of winter mixed layer depth (*black*), winter surface concentrations of iron (*magenta*), and summer surface concentrations of phytoplankton (*green*) for each year, averaged over regions in the Pacific (53–61°S, 143–150°W; *top*) and in the Atlantic (53–61°S, 18–24°W; *bottom*) sector of the ACC. The separate time series display 3–monthly running means of vertical velocity (w) in the respective areas

Peninsula. A simple relation between mixed-layer depth and phytoplankton concentrations cannot be detected in the Atlantic Sector of the ACC (including the Scotia Sea), where interannual variability of winter mixed-layer depth is considerably smaller. Again, phytoplankton concentrations are enhanced following increased iron concentrations (Fig. 4, bottom panel) but the amplitudes are significantly smaller than in the Pacific sector. Oceanic upwelling (Fig. 4, grey line) in the Atlantic sector of the ACC is stronger (mean: 0.038 m day^{-1}) than in the Pacific (0.018 m day^{-1}); iron supply in this region thus mainly occurs due to upwelling, not by entrainment at the mixed-layer base. We conclude that the variations of surface concentrations of dissolved iron and of primary production are significantly smaller than in the Pacific sector and are determined mainly by anomalies of vertical velocity.

Variations of zooplankton concentration are closely related to the anomalies of phytoplankton concentration (Fig. 3, bottom panel). Positive anomalies in phytoplankton concentration are associated with an enhanced growth of zooplankton. The maxima, however, are delayed by roughly 2 weeks.

Sensitivity studies with varied initial iron concentrations indicate that these findings are not sensitive to the initial iron concentration field. Phytoplankton concentrations change by roughly 10% when the initial iron concentrations are raised (or reduced) by 40%. However, the mechanisms for iron supply in the euphotic zone in the different sectors do not change, and the qualitative distribution of phytoplankton biomass is not affected.

3.2 Impact of sea ice – the Ronne Polynya

Oscillations associated with the ACW are visible not only in the ACC. Timmermann et al. (2002b) have shown that ACW-related anomalies of the meridional wind stress in the inner Weddell Sea create an interannual variability of sea-ice export. In the austral summer 1997/1998, extraordinarily strong winds from the southwest (Hunke und Ackley 2001) led to the development of a polynya in the southern Weddell Sea which is called the Ronne Polynya. In our simulation, the formation of a large area of open water in December/January 1997/1998 (Fig. 5, upper panels) leads to a large phytoplankton bloom in this usually ice-covered region (Fig. 5; lower left). The occurrence of the large phytoplankton bloom is consistent with SeaWIFS-derived remote sensing data (Moore and Abbott 2000). Quantitatively, the phytoplankton concentrations calculated from SeaWIFS data are in good agreement with the modelled field (Fig. 5; lower panels). Zooplankton quickly responds to the enhanced primary

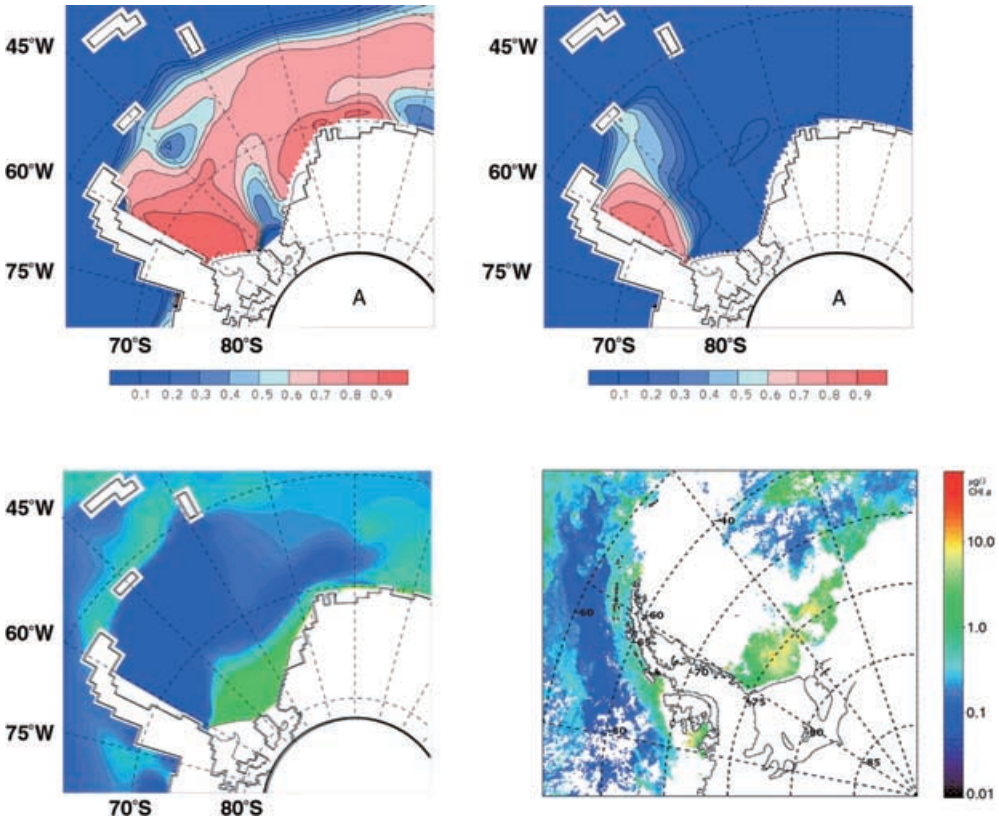

Fig. 5 Simulated mean sea-ice extent in December 1997 (*top left*) and January 1998 (*top right*); simulated mean surface chlorophyll concentration in January 1998 (μg l^{-1}) (*bottom left*) and mean surface chlorophyll concentration in January 1998, recorded from SeaWIFS (*bottom right*; Schwarz, personal communication), in the Weddell Sea

production and phytoplankton biomass, leading to an anomalously high standing stock of zooplankton biomass (not shown).

The spontaneous occurrence of a phytoplankton bloom in the Ronne Polynya indicates that ecosystem dynamics in the Southern Ocean is strongly influenced by the ice coverage. Strong signals of interannual variability are found in the continental shelf zones and in regions which are seasonally ice-covered (Fig. 6). While the maximum of solar irradiance occurs in December, sea-ice extent during early summer is still high. Phytoplankton blooms can only develop in regions of open water; as the location of early sea-ice breakup varies considerably from year to year, so does the location of plankton blooms in the inner Weddell Sea. Due to the corresponding absorption of light, interannual variations of sea-ice coverage cause significantly stronger fluctuations than the mixed-layer anomalies in the Pacific sector of the ACC or others regions north of the SIZ.

Another region of increased phytoplankton variability is found near Maud Rise, in the eastern Weddell Sea. Regional upwelling induced by passing cyclones is locally enhanced due to the presence of the seamount. Here, atmospheric variability on a synoptic scale creates local anomalies of phytoplankton biomass.[1]

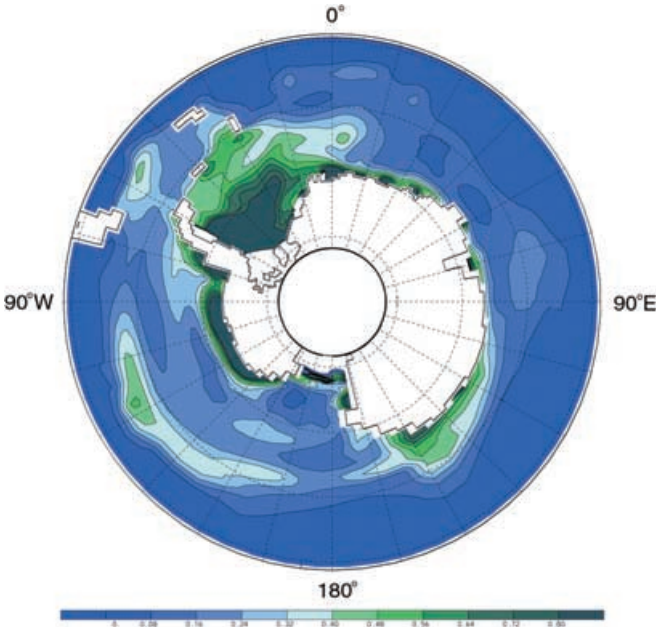

Fig. 6 Relative standard deviation of summer surface concentrations of phytoplankton (μg Chl a l^{-1}) in January 1985–2000

3.3 Primary production and carbon sequestration

Area-averaged primary production in the different sectors of the Southern Ocean (Table 1) ranges from 32 to 43 g C m^{-2} a^{-1}, agreeing well with calculations

[1] In the real ocean, tidal amplification at the seamount (Beckmann et al. 2001) may further contribute to an enhanced productivity near Maud Rise

Table 1 Area-averaged primary production [g C $m^{-2}a^{-1}$] south of 50°S of the Atlantic sector (63°W–20°E), Pacific sector (150°W–71°W), Ross Sea sector (150°W–150°E), Indian sector (20°E–150°E) and of the whole Southern Ocean.

Atlantic sector	36.9 ± 1.5
Pacific sector	32.2 ± 1.1
Ross Sea sector	37.9 ± 1.5
Indian sector	43.3 ± 1.6
Southern Ocean	38.1 ± 0.8

derived from carbon requirements of top predators, which are between 30 and 40 g C m^{-2} a^{-1} (Priddle et al. 1998). Regional differences in the productivity are coherent with estimates derived from satellite images and observations (Tréguer and Jaques 1992; Arrigo et al. 1998; Rubin et al. 1998): due to low iron concentrations, productivity in the Pacific sector is comparatively small. High phytoplankton concentrations in the Ross Sea (Sect. 3.1) are associated with a high productivity in this sector. In the Atlantic and Indian sectors, high productivity is confined to the Coastal and Continental Shelf Zone (CCSZ) and parts of the SIZ. It is partly counterbalanced by the low productivity in the iron-limited permanent open-ocean zone (POOZ), but as large parts of the CCSZ and SIZ in these sectors are ice-free for 3–4 months during the austral summer, annual mean productivity amounts to values equal to or even greater than the rates from the Ross Sea sector.

The effect of local interannual variability on circumpolar mean primary production is rather small. Total simulated primary production in the whole Southern Ocean (south of 50°S) is 1.7 GT C a^{-1} with a standard deviation of only 0.037 GT C a^{-1} (referring to an ensemble of annual means). Estimates of net CO_2 fluxes are in the order between 0.1 and 0.3 GT C a^{-1} (Takahasi et al. 1997; Rayner et al. 1999). Assuming that maximum 4% of primary production is exported into the deep ocean (Fischer et al. 2000), interannual variability of simulated primary production converts into fluctuations of carbon sequestration between 0.5 and 1.5%.

4 Summary

We have presented a newly developed circumpolar coupled ice–ocean–ecosystem model that includes biogeochemical cycles of nitrogen and silica and considers possible iron limitation. It is configured in a circumpolar domain between the Antarctic continent and 50°S. Consisting of a primitive-equation ocean model with a terrain-following vertical coordinate and a dynamic–thermodynamic sea-ice model, the physical component provides a realistic environment for the modelled ecosystem. The use of high-frequency forcing data ensures an adequate representation of atmospheric variability and sea-ice concentration fields on seasonal and interannual time scales.

Model results indicate that interannual variability of primary production is small compared to the long-term carbon sequestration of the Southern Ocean. However, on regional (and local) scales, atmospheric anomalies associated with the Antarctic Circumpolar Wave (ACW) strongly influence the ecosystem in the southern ACC and in parts of the Seasonal Ice Zone (SIZ). In the Pacific sector of the Southern Ocean, strongly varying winds and heat fluxes cause large anomalies of winter mixed-layer depth. Increased iron supply due to vigorous entrainment at the mixed-layer base during autumn and winter stimulates primary production in the subsequent summer, so that anomalously high phytoplankton concentrations are found 3–5 months after an anomalously deep winter mixed layer. In the Atlantic sector, however, interannual variability of primary production is less pronounced and mainly caused by fluctuations of oceanic upwelling. Again, an increased iron supply triggers positive anomalies of phytoplankton biomass. However, as the mechanisms for the enhancements of primary production differ between the Pacific and the Atlantic Sector of the ACC, the ACW induces regional oscillations of phytoplankton biomass in both sectors, but not a propagating signal.

Regional productivity in the individual sectors of the Southern Ocean differs due to characteristic differences in the physical regime: persistent oceanic upwelling mainly during the winter season, an early sea-ice breakup in the Ross Polynya and a shallow mixed layer in summer cause a high productivity and high phytoplankton concentrations in the Ross Sea. Outside the Ross Sea, high productivity is confined to the Coastal and Continental Shelf Zone (CCSZ) and those parts of the SIZ where an early breakup of sea ice allows for the development of a phytoplankton bloom in a shallow mixed layer. Light limitation due to the presence of sea ice prohibits phytoplankton blooms in large parts of the SIZ; ACW-related sea-ice anomalies like the Ronne Polynya of 1997/1998 may thus induce spontaneous phytoplankton blooms even very far south. We conclude that regional and interannual variations in physical parameters like wind, heat fluxes and ice coverage strongly influence the occurrence of phytoplankton blooms and that the mechanisms relevant for this interaction are not confined to the effects of a varying mixed-layer depth.

A relatively simple ecosystem model like BIMAP cannot cover all aspects of variability. Long-term observations from Elephant Island indicate that krill populations increase in years with a large ice extent, while in ''warm'' years krill abundance is low and salps dominate the community of swarm organisms (Loeb et al. 1997; Siegel et al. 1998). Given the large impact of atmospheric variability on sea-ice coverage, this would imply that fluctuations related to the ACW not only affect primary production and phytoplankton biomass but also induce shifts in species composition at higher trophical levels.

Acknowledgements Data of the ECMWF analysis and reanalysis were received via the DWD. The authors would like to thank Dr. Jill Schwarz for providing the SeaWIFS images. The comments of three anonymous reviewers helped to improve the manuscript.

Appendix A. The biological model BIMAP

BIMAP is designed as an ecosystem module for a three-dimensional prognostic ocean model. It comprises eight compartments: phytoplankton (P), zooplankton (Z), the nutrients nitrate (N_n), ammonium (N_a), silicate (Si) and iron (Fe), and detritus which is decomposed into a nitrogen part (D_N) and a silicium part (D_{Si}). We rate this as an ecosystem model of intermediate complexity: it is complex enough to cover a large part of the relevant processes but still concise, so it can be coupled to three-dimensional hydrodynamical models.

A.1 Model concept

The evolution of any biological tracer (T_b) is determined by the non-linear advection–diffusion equation

$$\frac{\partial T_b}{\partial t} + u \cdot \nabla T_b = \left(\frac{\partial T_b}{\partial t}\right)_b + \mathcal{D}^{T_b} \ , \tag{1}$$

which on the left-hand side features the local time derivative and the effect of advection. The first term on the right-hand side represents changes due to biological processes which are described below. Advection of biological tracers is computed from the simulated ocean currents u (u is the three-dimensional velocity vector); the divergence $\mathcal{D}^{T_b}$ of turbulent fluxes is parameterized using the time- and space-dependent ocean model diffusivities $v^{T(x,y,z,t)}$ with

$$\mathcal{D}^{T_b} = \nabla(v^T \nabla T_b) \ . \tag{2}$$

Coupled to the circumpolar ice-ocean model BRIOS-2 (Timmermann et al. 2002a), horizontal and vertical advection are computed using an explicit second-order finite differences scheme (Haidvogel and Beckmann 1999). Vertical turbulent transport of both oceanographic and biological tracers is parameterized using the Pacanowski and Philander (1986) mixing scheme. Lateral diffusivity is a function of the local Reynolds number.

A.2 Parameterization of biochemical fluxes

Phytoplankton

Biogenic changes in phytoplankton concentration (P) are described as

$$\left(\frac{\partial P}{\partial t}\right)_b = (1-\gamma)\cdot\sigma\cdot P - g_Z \cdot Z - \mu_P \cdot P \ , \tag{3}$$

where the terms on the right-hand side denote the primary production, the grazing by zooplankton and the natural mortality; γ is the exudation coefficient. The growth rate σ comprises the maximum (light-dependent) growth rate ω and a possible nutrient limitation η:

$$\sigma = \omega \cdot \eta \quad \text{with } 0 < \eta < 1 \ . \tag{4}$$

Using the law of minimum (Liebig 1840), η considers possible nutrient limitation by nitrate, silicate or iron:

$$\eta = \min\left(\frac{N_n}{k_{N_n}+N_n}, \frac{Si}{k_{Si}+Si}, \frac{Fe}{k_{Fe}+Fe}\right) \ . \tag{5}$$

A Michaelis-Menten type relation is assumed for all nutrients using the half-saturation constants k_{N_n}, k_{Si} and k_{Fe}. The light-dependent growth rate ω is described by

$$\omega = \frac{V_P \cdot \alpha \cdot I(z)}{\sqrt{V_P^2 + \alpha^2 \cdot I^2(z)}} \ , \tag{6}$$

where

$$I(z) = I_S \cdot \exp\left(\int_0^z -\left[k_w + k_c \cdot P(z')\right] \mathrm{d}z'\right) \tag{7}$$

is the intensity of the photosynthetic active radiation (PAR) in a depth z below the surface (Evans and Parslow 1985; Fasham et al. 1990). For the conversion from solar radiation to PAR we use a factor of 43% according to Jerlov (1976) and Jitts et al. (1976). As the Southern Ocean belongs to oceanic type I (Jerlov 1976; Bracher and Tilzer 2001), we choose $k_w = 0.04\ \mathrm{m}^{-1}$ (Lorenzen 1972) as the attenuation coefficient of seawater. The self-shading parameter k_c and the initial slope α of the PI curve were derived from cruise measurements during the SO-JGOFS cruise ANT XIII/2 (Bracher et al. 1999). Parameter values are given in Table 2.

Table 2 Parameter values and references

1. Phytoplankton	
Initial slope of the PI curve (Bracher et al. 1999)	$\alpha = 0.027 \frac{m^2}{W\,\mathrm{day}^{-1}}$
Self-shading parameter (Bracher et al. 1999)	$k_c = 0.07 \frac{m^2}{mmol}$
Maximum growth rate (Eppley 1972)	$V_P = 1.2 \frac{1}{\mathrm{day}}$
Mortality rate (Hense et al. 2000)	$\mu_P = 0.05 \frac{1}{\mathrm{day}}$
Half-saturation constant for silicate (Nelson and Tréguer, 1992)	$k_{Si} = 4.6 \frac{mmol}{m^3}$
Half-saturation constant for nitrate (Sommer 1986)	$k_{N_i} = 0.3 \frac{mmol}{m^3}$
Half-saturation constant for ammonium	$k_{N_a} = 0.3 \frac{mmol}{m^3}$
Half-saturation constant for iron (Landry et al. 1997)	$k_{Fe} = 0.12 \frac{\mu mol}{m^3}$
Exudation coefficient (Williams 1990)	$\gamma = 0.05$
2. Zooplankton	
Assimilation efficiency (Schnack 1985)	$\beta = 0.67$
Excretion rate (Huntley and Nordhausen 1995)	$\varepsilon = 0.0078 \frac{1}{d}$
Mortality rate (Hense et al. 2000)	$\mu z = 2.0 \frac{m^3}{mmol\,\mathrm{day}^{-1}}$
3. Nutrients	
Si:N uptake ratio (Hense et al. 2002)	$r_{Si} = 2$
Fe:N uptake ratio (Sarthou et al. 1997)	$r_{Fe} = 2.65 \times 10^{-5}$
4. Detritus	
Silica dissolution rate (Tréguer et al. 1989)	$\tau_{Si} = 0.018 \frac{1}{\mathrm{day}}$
Remineralization rate (Biddanda 1988)	$\tau_{N_a} = 0.07 \frac{1}{\mathrm{day}}$

The exudation of dissolved organic nitrogen (DON) during the cell division is parameterized as $\gamma \cdot \sigma \cdot P$ and is directly led into the ammonium pool.

Zooplankton

The zooplankton (Z) equation considers grazing and the mortality (μ_Z) and excretion (ε) rates using

$$\left(\frac{\partial Z}{\partial t}\right)_b = \beta \cdot g_Z \cdot Z - \mu_Z \cdot Z^2 - \varepsilon \cdot Z \ , \tag{8}$$

where $\beta \cdot g_Z \cdot Z$ gives the growth of zooplankton biomass due to grazing while $(1-\beta) \cdot g_Z \cdot Z$ is the part of ingested food which is excreted as faecal pellets. The grazing rate g_Z has been calculated from experiments with the abundant herbivorous copepod species *Calanoides acutus* (Schnack 1985) and reads

$$g_Z = 4.5 \cdot 10^{-4}\,\mathrm{day}^{-1} \cdot \left(79.5 \frac{\mathrm{m}^3}{\mathrm{mmol}} \cdot P\right)^{1.3} \tag{9}$$

(Hense et al. 2000). While the excretion is assumed to be proportional to Z, mortality is parameterized as a quadratic function of zooplankton concentration.

Nutrients

Biogenic changes of the nutrient concentrations (N_n, N_a, Si, Fe) are due to uptake by phytoplankton $\sigma \cdot P$, exudation $\gamma \cdot \sigma \cdot P$, excretion $\varepsilon \cdot Z$ and remineralization τD. Although we do not allow ammonium supply to limit phytoplankton growth, the uptake ratio between ammonium and nitrate is determined using the concentrations N_a and N_n, and the half-saturation constants k_{N_a} and k_{N_n}:

$$\left(\frac{\partial N_\mathrm{n}}{\partial t}\right)_b = -\sigma \cdot \frac{\frac{N_\mathrm{n}}{k_{N_\mathrm{n}}+N_\mathrm{n}}}{\frac{N_\mathrm{n}}{k_{N_\mathrm{n}}+N_\mathrm{n}} + \frac{N_\mathrm{a}}{k_{N_\mathrm{a}}+N_\mathrm{a}}} \cdot P \tag{10}$$

$$\left(\frac{\partial N_\mathrm{a}}{\partial t}\right)_b = -\sigma \cdot \frac{\frac{N_\mathrm{a}}{k_{N_\mathrm{a}}+N_\mathrm{a}}}{\frac{N_\mathrm{n}}{k_{N_\mathrm{n}}+N_\mathrm{n}} + \frac{N_\mathrm{a}}{k_{N_\mathrm{a}}+N_\mathrm{a}}} \cdot P + \gamma \cdot \sigma \cdot P + \varepsilon \cdot Z + \tau_{N_\mathrm{a}} D_\mathrm{N} \tag{11}$$

$$\left(\frac{\partial \mathrm{Si}}{\partial t}\right)_b = -r_\mathrm{Si} \cdot \sigma \cdot P + \tau_\mathrm{Si} D_\mathrm{Si} \tag{12}$$

$$\left(\frac{\partial \mathrm{Fe}}{\partial t}\right)_b = -r_\mathrm{Fe} \cdot \sigma \cdot P. \tag{13}$$

Following studies with an eddy-resolving model version (Hense et al., personal communication 2002), we conduct the experiment with a molar Si/N uptake ratio $r_\mathrm{Si} = 2$.

As quantitative knowledge about the time scales involved is not available, we neglect iron remineralization. Thus, biology acts only as a sink for iron, while the only source is advection and diffusion from the deep ocean.

Iron/carbon uptake ratios have been derived from measurements in the Indian sector of the Southern Ocean by Sarthou et al. (1997). Using the Redfield ratio between carbon and nitrogen, we converted their estimates to $r_\mathrm{Fe} = 2.65 \times 10^{-5}$ [mol/mol]. For iron limitation, we use a half-saturation constant $k_\mathrm{Fe} = 0.12\ \mathrm{nmol\,l^{-1}}$ which is in agreement with observations (Landry et al. 1997) and follows the analysis of sensitivity studies (Hense et al. 2002).

Detritus

The detritus pool is decomposed into a nitrogen part D_N and a silica part D_Si. Biogenic evolution of these compartments follows the equations

$$\left(\frac{\partial D_\mathrm{N}}{\partial t}\right)_b = \mu_P \cdot P + \mu_Z \cdot Z + (1-\beta) \cdot g_Z \cdot Z - r_{l_\mathrm{N}} \tau_{N_\mathrm{a}} D_\mathrm{N} \tag{14}$$

$$\left(\frac{\partial D_\mathrm{Si}}{\partial t}\right)_b = (\mu_P \cdot P + \mu_Z \cdot Z + g_Z \cdot Z) \cdot r_{Si} - r_{l_{Si}} \tau_{Si} D_{Si} \ , \tag{15}$$

and includes mortality of phyto- and zooplankton, production of faecal pellets and remineralization with the time scales τ_{N_a} and τ_Si (Hense et al., 2000).

Following observations and results from model experiments indicating that roughly 50% of the produced biogenic silica and 80% of particulate organic nitrogen are remineralized in the upper water column while the rest of it sinks down to the deeper ocean (Nelson et al. 1995; Pondaven et al. 1999), detritus loss and remineralization fluxes are linked by a factor of 2 for silica and a factor of 1.25 for nitrogen-based detritus (Hense et al., personal communication 2002). We use these numbers for the loss-to-remineralization ratios r_{l_Si} and r_{l_N}, respectively.

Initialization and boundary conditions

The nutrients silicate and nitrate are initialized using data from the WOCE dataset. Due to the lack of gridded data, iron concentration is initialized using the vertical profile

$$Fe^{t=0}(z) = 1.2 \times 10^{-3}\,\mathrm{mmol\,m^{-3}} + 0.45 \times 10^{-6}\,\mathrm{mmol\,m^{-4}}|z| \ , \tag{16}$$

which fits to iron concentrations at the surface and at the bottom derived from measurements in the Southern Ocean (Löscher et al. 1997; Sohrin et al. 2000; de Baar and de Jong 2001). As remineralization below the euphotic zone is not explicitly considered, a restoring to the initial values of iron, nitrate and silicate with a time scale of 1 year is applied in the bottom layer.

At the northern boundary, $\nabla T_b = 0$ is applied. For the solar radiation the daily and annual cycles as well as the latitude and mean cloud cover, using the standard astronomical formulae of Zillmann (1972) and Laevastu (1960), are considered.

References

Arrigo KR, Worthen D, Schnell A, & Lizotte MP (1998) Primary production in Southern Ocean waters. J Geophys Res 103(C8): 15587–15600

Beckmann A, Hellmer HH, Timmermann R (1999) A numerical model of the Weddell Sea: large-scale circulation and water-mass distribution. J Geophys Res 104/C10: 23375–23391

Beckmann A, Timmermann R (2001) Circumpolar influences on the Weddell Sea: indication of an Antarctic Circumpolar Coastal Wave. J Climate 14: 3785–3792

Beckmann A, Timmermann R, Pereira AF, Mohn C (2001) The effect of flow at Maud Rise on the sea-ice cover – numerical experiments. Ocean Dynamics 52: 11–25

Biddanda BA (1988) Microbial aggregation and degradation of phytoplankton-derived detritus in seawater. II. Microbial metabolism. Mar Ecol Prog Ser 42: 89–95

Bracher AU, Kroon BMA, Lucas MI (1999) Primary production, physiological state and composition of phytoplankton in the Atlantic sector of the Southern Ocean. Mar Ecol Prog Ser 190: 1–16

Bracher AU, Tilzer MM (2001) Underwater light field and phytoplankton absorbance in different surface water masses of the Atlantic sector of the Southern Ocean. Polar Biol 24/9: 687–696

de Baar HJW, de Jong JTM (2001) Distributions, sources and sinks of iron in seawater. In: Turner DR, Hunter KA (eds) The biogeochemistry of iron in seawater. pp 123–253

Eppley RW (1972) Temperature and phytoplankton growth in the sea. Fish Bull 70: 1063–1085

Evans GT, Parslow JS (1985) A model of annual plankton cycles. Biol Oceanogr 3: 327–347

Fasham MJR, Ducklow HW, McKelvie SM (1990) A nitrogen-based model of plankton dynamics in the oceanic mixed layer. J Mar Res 48: 591–639

Fischer G, Ratmeyer V, Wefer G (2000) Organic carbon fluxes in the Atlantic and the Southern Ocean: relationship to primary production compiled from satellite radiometer data. Deep-Sea Res II, 47(9–11): 1961–1997

Haidvogel DB, Beckmann A (1999) Numerical Ocean Circulation Modelling. Imperial College Press, London 344 pp

Haidvogel DB, Wilkin JL, Young RE (1991) A semi-spectral primitive equation ocean circulation model using vertical sigma and orthogonal curvilinear horizontal coordinates. J Comput Phys 94: 151–185

Hense I, Bathmann UV, Timmermannm R (2000) Plankton dynamics in frontal systems of the Southern Ocean. J Mar Syst 27/1–3: 235–252

Hibler III, WD (1979) A dynamic thermodynamic sea ice model. J Phys Oceanogr 9(4): 815–846

Hunke EC, Ackley SF (2001) A numerical investigation of the 1997-1998 Ronne Polynya. J Geophys Res, 106(C10): 22373–22382

Huntley ME, Nordhausen W (1995) Ammonium cycling by Antarctic zooplankton in winter. Mar Biol 121: 457–467

Jerlov NG (1976) Marine optics. Elsevier, Newyork

Jitts HR, Morel A, Saijo Y (1976) The relation of oceanic primary production to available photosynthetic irradiance. Aust J Mar Fresh Res 27: 441–454

Kahru M, Mitchell BG (1999) Empirical chlorophyll algorithm and preliminary SeaWIFS validation for the California Current. Int J Remote Sensing 20/17: 3423–3429

Kudela RM, Chavez FP (1998) Changes in phytoplankton structure during the 1997–1998 El Ninño in Central California. SPIE Ocean Optics, 00XIV Kailua-Kona, Hawaii

Laevastu T (1960) Factors affecting the temperature of the surface layer of the sea. Comment Phys Math 25/1

Landry MR et al. (1997) Iron and grazing constraints on primary production in the central equatorial Pacific: an EqPac synthesis. Limnol Oceanogr, 42/3: 405–418

Liebig von J (1840) Organic chemistry and its application to agriculture and physiology. Taylor and Walton, London

Le Quéré C, Orr JC, Monfray P, Aumont O, Madec G (2000) Interannual variability of the oceanic sink of CO_2 from 1979 through 1997. Global Biogeochem Cycles 14: 1247–1265

Loeb V, Siegel V, Holm-Hansen O, Hewitt R, Fraser W, Trivelpiece W, Trivelpiece S (1997) Effects of sea-ice extent and krill or salp dominance on the Antarctic food web. Nature 387/6636: 897–900

Löscher BM, de Baar HJW, de Jong JTM, Veth C (1997) The distribution of Fe in the Antarctic Circumpolar Current. Deep-Sea Res II, 44(1–2): 143–187

Lorenzen CJ (1972) Extiction of light in the ocean by phytoplankton. J Cons 34: 262–267

Moore JK, Abbott MR (2000) Phytoplankton chlorophyll distributions and primary production in the Southern Ocean. J Geophys Res 105(C12): 28709–28722

Nelson DM, Tréguer P (1992) Role of silicon as a limiting nutrient to Antarctic diatoms: evidence from kinetic studies in the Ross Sea ice-edge zone. Mar Ecol Prog Ser 80: 255–264

Nelson DM, Tréguer P, Brzezinski MA, Leynaert A, Quéguiner B (1995) Production and dissolution of biogenic silica in the ocean: revised global estimates, comparison with regional data and relationship to biogenic sedimentation. Global Biogeochem Cycle 9/3: 359–372

Olbers D, Gouretski V, Seiss G, Schröter J (1992) Hydrographic atlas of the Southern Ocean. Alfred Wegener-Institut für Polar- und Meeresforschung, Bremerhaven

Pacanowski RC, Philander SGH (1986) A model of the seasonal cycle in the tropical Atlantic Ocean. J Geophys Res 91: 14192–14206

Pondaven P, Ruiz-Pino D, Druon JN, Fravalo C, Tréguer P (1999) Factors controlling silicon and nitrogen biogeochemical cycles in high-nutrient, low chlorophyll systems (the Southern Ocean and the North Pacific): comparison with a mesotrophic system (the North Atlantic). Deep-Sea Res 46: 1923–1968

Priddle J, Boyd IL, Whitehouse MJ, Murphy EJ, Croxall JP (1998) Estimates of Southern Ocean primary production – constraints from predator carbon demand and nutrient drawdown. J Mar Systems 17(1–4): 275–288

Rayner PJ, Enting IG, Francey RJ, Langenfelds R (1999) Reconstructing the recent carbon cycle from atmospheric CO_2, $\delta\,^{13}C$ and O_2/N_2 observations. Tellus 51B: 213–232

Rubin SI, Takahashi T, Chipman DW, Goddard JG (1998) Primary productivity and nutrient utilization ratios in the Pacific sector of the Southern Ocean based on seasonal changes in seawater chemistry. Deep-Sea Res I, 45(8): 1211–1234

Sarthou G, Jeandel C, Brisset L, Amouroux D, Besson T, Donard OFX (1997) Fe and H_2O_2 distributions in the upper water column in the Indian sector of the Southern Ocean. Earth Planet Sci Lett 147: 83–92

Schnack SB (1985) Feeding by *Euphausia superba* and copepod species in response to varying concentrations of phytoplankton. In: Siegfried WR, Condy PR, Laws RM (eds). Antarctic nutrient cycles and food webs Springer 311–323

Siegel V, Loeb V, Groeger J (1998) Krill (*Euphausia superba*) density, proportional and absolute recruitment and biomass in the Elephant Island region (Antarctic Peninsula) during the period 1977 to 1997. Polar Biol 19/6: 393–398

Sohrin Y et al. (2000) The distribution of Fe in the Australian sector of the Southern Ocean. Deep-Sea Res I, 47: 55–84

Sommer U (1986) Nitrate and silicate competition among antarctic phytoplankton. Mar Biol 91: 345–351

Takahashi T. et al. (1997) Global air–sea flux of CO_2: an estimate based on measurements of sea–air pCO_2 difference. Proceedings of the National Academy of Sciences, USA 94: 8929–8299

Timmermann R, Beckmann A, Hellmer HH (2002a) Simulation of ice–ocean dynamics in the Weddell Sea part I. Model description and validation. J Geophys Res 107 (C3): 10.1029/2000JC000741

Timmermann R, Hellmer HH, Beckmann A (2002b) Simulation of ice–ocean dynamics in the Weddell Sea part II. Interannual variability 1985–1993. J Geophys Res 107 (C3): 10.1029/2000JC000742

Tréguer J, Jacques G (1992) Dynamics of nutrients and phytoplankton, and fluxes of carbon, nitrogen and silicon in the Antarctic Ocean. Polar Biol 12: 149–162

Tréguer J, Kamatami A, Gueneley S, Quéguiner B (1989) Kinetics of dissolution of Antarctic diatoms frustules and the biogeochemical cycle of silicon in the Southern Ocean. Polar Biol 9: 397–403

White BW, Peterson RG (1996) An Antarctic circumpolar wave in surface pressure, wind, temperature and sea-ice extent. Nature 380(6576): 699–702

Williams PJ (1990) The importance of losses during microbial growth: commentary on the physiology, measurement and ecology of the release of dissolved organic material. Mar Microb Food Webs 4: 175–206

WOCE Hydrographic Program Office Special Analysis Center (1997) http://www.dkrz.de/ u241046/SACserver/SACHome.htm

Zillmann JW (1981) A study of some aspects of the radiation and heat budgets of the Southern Hemisphere oceans. In: Meteorological study, 26, Bureau of Meteorology, Dept of the Interior, Canberra, Australia, 526 pp